Detecting fluid signals in seismicity data through statistical earthquake modeling

Sebastian Hainzl
Institute of Geo Sciences, University of Potsdam, Potsdam, Germany

Yosihiko Ogata
Institute of Statistical Mathematics, Tokyo, Japan

Received 21 June 2004; revised 25 August 2004; accepted 27 August 2004; published 4 March 2005.

[1] According to the well-known Coulomb failure criterion the variation of either stress or pore pressure can result in earthquake rupture. Aftershock sequences characterized by the Omori law are often assumed to be the consequence of varying stress, whereas earthquake swarms are thought to be triggered by fluid intrusions. The role of stress triggering can be analyzed by modeling solely three-dimensional (3-D) elastic stress changes in the crust, but fluid flows which initiate seismicity cannot be investigated without considering complex seismicity patterns resulting from both pore pressure variations and earthquake-connected stress field changes. We show that the epidemic-type aftershock sequence (ETAS) model is an appropriate tool to extract the primary fluid signal from such complex seismicity patterns. We analyze a large earthquake swarm that occurred in 2000 in Vogtland/NW Bohemia, central Europe. By fitting the stochastic ETAS model, we find that stress triggering is dominant in creating the observed seismicity patterns and explains the observed fractal interevent time distribution. External forcing, identified with pore pressure changes due to fluid intrusion, is found to directly trigger only a few percent of the total activity. However, temporal deconvolution indicates that a pronounced fluid signal initiated the swarm. These results are confirmed by our analogous investigation of model simulations in which earthquakes are triggered by fluid intrusion as well as stress transfers on a fault plane embedded in a 3-D elastic half-space. The deconvolution procedure based on the ETAS model is able to reveal the underlying pore pressure variations.

Citation: Hainzl, S., and Y. Ogata (2005), Detecting fluid signals in seismicity data through statistical earthquake modeling, *J. Geophys. Res.*, *110*, B05S07, doi:10.1029/2004JB003247.

1. Introduction

[2] Stress triggering has been identified as an important mechanism for aftershock sequences [*Stein*, 1999]. This mechanism is based on a well-known criterion for earthquake occurrence, the Coulomb failure criterion [*Harris*, 1998],

$$\mathrm{CFS} \equiv \tau - \mu(\sigma - P) \geq 0 \tag{1}$$

stating that a positive Coulomb failure stress (CFS) could promote failures. Here, τ defines the shear and σ the normal stress on the failure plane (positive for compression), and μ is the coefficient of friction. In the presence of fluids, the pore pressure P has to be taken into account. The $(\sigma - P)$ term is known as the effective normal stress.

[3] The activity rate λ of aftershock sequences generally decays according to the modified Omori law, $\lambda(t) = K(c + t)^{-p}$, where K, c and p are constants, and t is the elapsed time since the main event [*Utsu et al.*, 1995]. The epidemic-type aftershock sequences (ETAS) model is a stochastic point process incorporating the empirically observed characteristics of stress triggered activity, where each earthquake has some magnitude-dependent ability to trigger its own Omori law type aftershocks [*Ogata*, 1988, 1993; *Helmstetter and Sornette*, 2002]. In particular, the rate of aftershocks induced by an earthquake that occurred at time t_i with magnitude M_i is given by

$$\lambda_i(t) = \frac{K_0}{(c + t - t_i)^p} e^{\alpha(M_i - M_{\min})} \tag{2}$$

for time $t > t_i$. The parameters K_0, α, c and p are constant to all earthquakes of a given area and $M_{\min}$ is the lowest magnitude cut of the catalog. The total occurrence rate,

$$\lambda(t) = \lambda_0 + \sum_{\{i:t_i<t\}} \lambda_i(t) \tag{3}$$

is sum of the rate of all preceding earthquakes and a constant background rate λ_0. Note that we use here the

0148-0227/05/2004JB003247$09.00

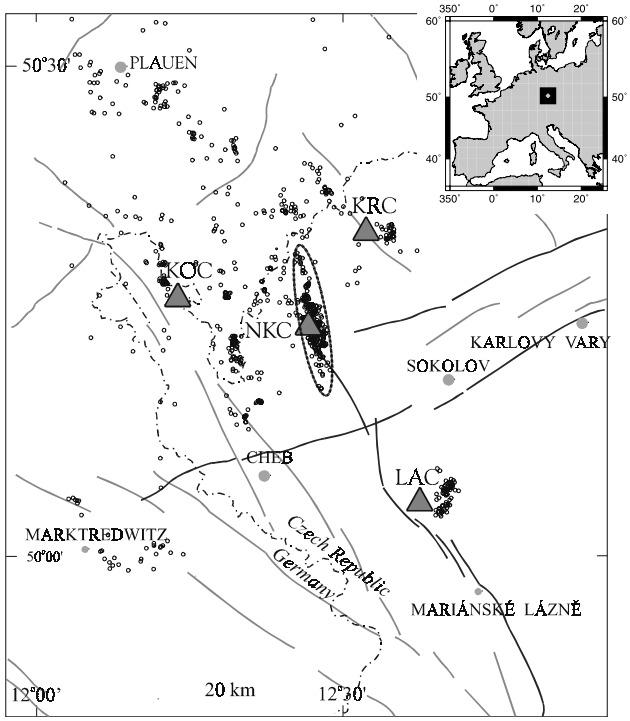

Figure 1. Map of the location of the Vogtland/NW Bohemia earthquake swarm region and its fault structure (line segments). Earthquake epicenters are indicated by circles, and the main swarm area is marked by the ellipse enclosing the year 2000 swarm activity.

symbol λ_0 instead of the commonly used μ to avoid confusion with the coefficient of friction. This background rate λ_0 refers to activity which is not triggered by precursory earthquakes, or in other words, which is not a part of an aftershock sequence. At tectonic plate boundaries, λ_0 is usually assumed to result from stress accumulation due to tectonic plate motion.

[4] The Coulomb failure criterion also explains earthquake clustering initiated by pore pressure variations. Fluids are often assumed to trigger earthquake swarm activity, which differs significantly in its temporal clustering and energy release from aftershock sequences [*Nur*, 1974; *Scholz*, 2002]. However, earthquakes induced by fluids themselves produce local stress field changes. Thus the mechanism of fluid triggering is always accompanied by stress triggering. However, fluid induced seismicity can also be described by the ETAS model, because it deals with internally (stress) triggered as well as externally forced events. In this case, the background rate λ_0 refers to activity forced by pore pressure changes instead of the movement of tectonic plates.

[5] In this study, we investigate the complex seismicity pattern of an earthquake swarm that occurred in 2000 in Vogtland/NW Bohemia, central Europe (see Figure 1). This region is well known for its episodic occurrence of earthquake clusters consisting of small magnitude events (*Jentzsch et al.* [2003] and papers in the same special issue). Although there is no active volcanism, CO_2 emanations present in this region are assumed to originate from degassing of an active magma body in the upper mantle [*Weinlich et al.*, 1999]. The correlation of the isotopic content of these gasses with swarm activity has led to the conclusions that the swarm activity is induced by fluid overpressure [*Brauer et al.*, 2003]. On the other hand, the fluid signal is not obvious in the seismicity pattern and the earthquake sequences have features in common with tectonic earthquake clusters (section 2). We show that the main characteristics of this swarm activity can be reproduced by model simulations in which earthquakes are triggered by fluid intrusion as well as stress transfers (section 3). In section 4, we analyze both the Vogtland swarm seismicity and model simulations by means of the ETAS model in order to extract the underlying fluid signal and demonstrate the efficiency of the method.

2. Vogtland Earthquake Swarm

[6] The earthquake swarm analyzed in this study occurred between August and December 2000 in the Novy Kostel focal area (Figure 1). It is the most recent and best documented strong earthquake swarm in Vogtland/NW Bohemia. The investigated earthquake catalog is recorded by the WebNET local seismic network [*Horalek et al.*, 2000] and consists of more than 8400 earthquakes with local magnitude $M_L \geq -0.5$ [*Fischer*, 2003]. The catalog is found to be complete for $M_L \geq 0.2$ [*Hainzl and Fischer*, 2002]. Thus we restrict our investigations to the $N = 4823$ earthquakes with magnitudes ≥ 0.2. The earthquakes are shown in Figure 2 as a function of their occurrence times.

[7] From previous investigations of this earthquake swarm [*Hainzl and Fischer*, 2002; *Fischer*, 2003], it is known that (1) all the earthquakes occur approximately on the same fault plane; (2) the spatial spreading of the swarm activity scales with the cumulative seismic moment release according to the theoretical relation for a crack growth $M_0 \sim R^3$ [*Scholz*, 2002], but the space-time pattern is complex; (3) the average seismic moment release increases during the swarm evolution according to $\langle M_0 \rangle \propto i^{1/4}$, where i is the earthquake index; and (4) the temporal occurrence is fractal (clustered on all timescales), in particular, the interevent time distribution can be described by the power law $t^{-1.5}$.

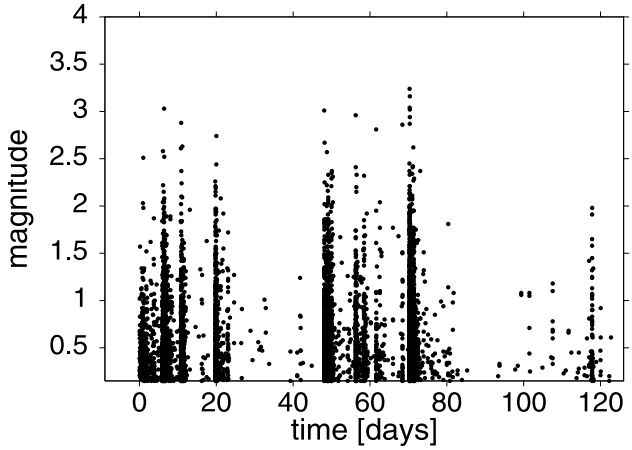

Figure 2. Local magnitudes of the Vogtland swarm earthquakes as a function of their occurrence. The time is measured from 28 August 2000.

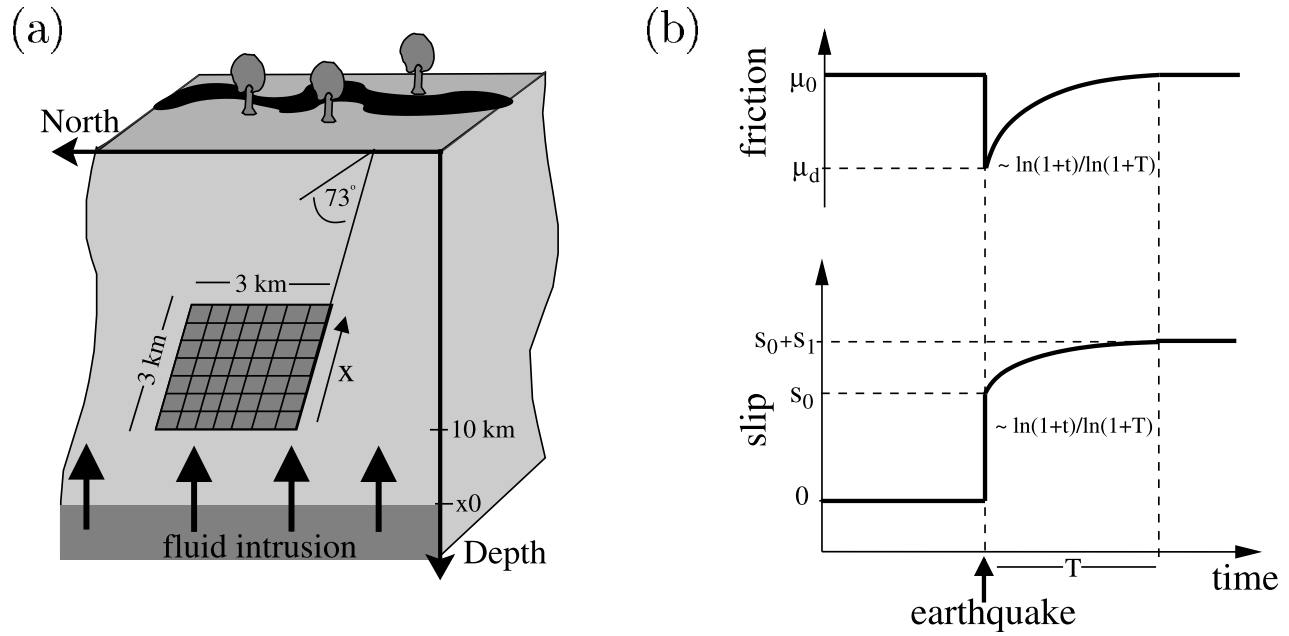

Figure 3. (a) Illustration of the model configuration and (b) assumed healing and slip characteristics.

Furthermore, embedded aftershock sequences have been identified [*Hainzl and Fischer*, 2002; *Hainzl*, 2003].

3. Simulated Swarm Activity

[8] In addition to the Vogtland swarm, we investigate earthquake catalogs resulting from the physical fault model proposed by *Hainzl* [2004]. After briefly introducing the model (section 3.1), we show the main characteristics of the simulations in section 3.2.

3.1. Physical Model

[9] The analyzed model [*Hainzl*, 2004] has been introduced to simulate seismicity patterns initiated by fluid migration in a narrow, porous, planar fault zone embedded in a three-dimensional (3-D) elastic half-space. For the most part, it is identical to the model proposed by *Yamashita* [1997, 1998] but with an added mechanism of postseismic creep on the fracture zone which leads to realistic aftershock activity according to the Omori law.

[10] Because the general description of the model is given elsewhere [*Yamashita*, 1997, 1998; *Hainzl*, 2004], we only give a brief summary and specify the parameter values used for our simulations here.

[11] The model is illustrated in Figure 3a. The fault plane of the Vogtland earthquake swarm is adapted by a 3 km $\times$ 3 km rectangular fault patch dipping 73°. The lower edge of the brittle segment is set to 10 km depth [*Hainzl and Fischer*, 2002]. This patch is discretized in 50 $\times$ 50 cells each of dimension 60 m $\times$ 60 m. The normal stress σ, the pore pressure P and the static coefficient of friction μ are assumed to be initially constant on the fault plane. The effective normal stress $\sigma - P$ is arbitrarily set to 25 MPa and the coefficient of friction is initially set to $\mu = 0.6$. The normal stress is assumed to remain constant during the simulation. Thus the effective stress only varies in response to pore pressure changes.

[12] Slip on a cell occurs if the Coulomb failure criterion (equation (1)) is fulfilled. The coseismic sliding is governed by a static/kinetic friction law [*Ben-Zion and Rice*, 1993]. If sliding is initiated, the coefficient of friction, i.e., the frictional resistance, drops to its lower dynamic value μ_d and remains there until the earthquake is terminated. The dynamic weakening of the fault strength is accompanied by a stress drop. The shear stress τ drops to the arrest stress τ_a which is smaller than the frictional dynamic stress μ_d $(\sigma - p)$ because of dynamic overshoot. To account for heterogeneities of the brittle properties, the values of τ_a and μ_d vary in space. The arrest stresses τ_a are uniformly distributed in the arbitrarily chosen interval between 2 and 8 MPa; the dynamic coefficient of friction varies between $\tau_a/25$ MPa and 0.6.

[13] The stress change at the fault plane due to relative slip of one segment is calculated with the analytic solution given by *Okada* [1992], where slip is in the strike direction and the half space rigidity is assumed to be 30 GPa [*Kurz et al.*, 2003].

[14] The sliding of one cell can lead to an instability in other cells and so on. An earthquake ends when all cells are stable with regard to the Coulomb failure criterion (equation (1)). The duration of earthquakes is much shorter than the typical time separating subsequent earthquakes. Thus we assume instantaneous coseismic slip, or in other words, that the whole earthquake occurs at the same time.

3.1.1. Healing and Postseismic Creep

[15] To account for logarithmic healing after coseismic slip observed in laboratory experiments [*Dieterich*, 1972; *Ruina*, 1983; *Scholz*, 1998], the fault strength is assumed to recover according to

$$\mu(\Delta t) = \mu_d + (\mu_0 - \mu_d)\frac{\log(1+\Delta t)}{\log(1+T)} \tag{4}$$

where T is the time interval required for complete healing and Δt is the time in minutes elapsed since the earthquake occurred (Figure 3b).

[16] It is known from laboratory experiments that the logarithmic healing results from asperity creep on the fracture zone, which leads to an increase of the contact area [*Scholz and Engelder*, 1976]. The model assumes that, after coseismic slip, the dislocation slowly extends due to creep on the earthquake rupture area, adapting observed afterslip characteristics in a simplified way [*Burgmann et al.*, 2002]. It is straightforward to assume that the afterslip is correlated to the strength; that is, slip is assumed to logarithmically increase according to

$$s(\Delta t) = s_0 + s_1 \frac{\log(1+\Delta t)}{\log(1+T)} \tag{5}$$

where s_0 and s_1 refer to the coseismic and postseismic slip. The fraction of postseismic slip $\kappa \equiv s_1/(s_0 + s_1)$ is a parameter in our simulations. The assumed slip characteristic is illustrated in the lower part of Figure 3b.

3.1.2. Fluid Diffusion

[17] According to Darcy's law, pore pressure variations in the fault plane due to an intrusion of fluids from a high-pressure source can be described by the diffusion equation

$$\frac{\delta}{\delta t} P = D \frac{\delta^2}{\delta x^2} P \tag{6}$$

where D is the hydraulic diffusivity [*Shapiro et al.*, 1997; *Yamashita*, 1997]. The diffusivity of the crust is generally expected to be between 0.01 and 10 m^2/s [*Scholz*, 2002]. The model assumes a high-pressure source which starts to release fluids at depth x_0. This source is assumed to be large and laterally extensive, thus the one-dimensional version of equation (6) can be solved to find deviations from the initially constant pressure state.

[18] Slip and strength evolution, as well as the pore pressure, diffusion are simulated by means of a finite difference scheme.

3.2. Characteristics

[19] The mean stress level of the initial stress field is found to determine whether the fault segment is in a subcritical, critical or supercritical state [*Hainzl*, 2004]. Similar to the results found for slider-block models [*Hainzl and Zöller*, 2001], earthquake ruptures occurring in overstressed (supercritical) faults cannot be stopped after growing beyond a critical size. This results in earthquake sequences characterized by a single dominant earthquake. Swarm-like activity occurs for initially subcritical stress states if the pore pressure increase is sufficient to bring the fault close to the critical state.

[20] We analyze model simulations with different combinations of the model parameters: (1) diffusivity D, (2) depth of the fluid source x_0, (3) pore pressure increase ΔP, (4) healing time T, and (5) fraction of postseismic creep κ. Although the simulations vary somewhat for different settings, the overall characteristics are almost independent of the parameter values and in very good agreement with the natural swarm occurrence in Vogtland. Figure 4 illustrates the main characteristics for one example, where the parameters are set to $D = 1.0\ m^2/s$, $x_0 = 10$ km, $\Delta P = 2$ MPa, $T = 0.1$ days, and $\kappa = 0.3$: The activity is not dominated by one large event, instead it occurs in several subclusters separated in space and time (Figure 4a). Of particular importance, the temporal occurrence of earthquakes is fractal, where the interevent time distribution reproduces the empirically observed power law $\sim t^{-1.5}$ (Figure 4b). The frequency-magnitude distribution can be fitted by a similar Gutenberg-Richter law (Figure 4c). We calculate for each event a local magnitude M_L from its seismic moment M_0 (in N m) by means of the empirical relation for the Vogtland region, $M_L = 0.95 \log(M_0) - 10.76$ [*Hainzl and Fischer*, 2002]. The shape of the resulting frequency-magnitude distribution is very similar to that of the Vogtland swarm earthquakes, and in particular the b value is the same. Note that the lower magnitude cutoff $\sim$0.8 is due to the subfault cell dimension of 60 m $\times$ 60 m. The seismic moment, which is on average released per event, monotonously increases during the evolution of the earthquake swarm according to $M_0 \sim i^{0.25}$, where i is the earthquake index (Figure 4d). Equivalently, the cumulative seismic moment release increases as $\Sigma M_0 \sim i^{1.25}$. Exactly, the same relation has been found for the Vogtland earthquake swarm [*Hainzl and Fischer*, 2002].

[21] On basis of these observations indicating clustered activity, we try to fit the ETAS model in order to separate the signals of stress triggering and external forcing in both observed and simulated data.

4. ETAS Modeling

[22] The estimation of the five parameters (λ_0, K_0, α, c, p) of the ETAS model (equation (3)) is carried out by the maximum likelihood method. The log likelihood with respect to the occurrence times of the earthquakes t_i is given by

$$\ln L(\lambda_0, K_0, c, \alpha, p) = \sum_{i=1}^{N} \ln \lambda(t_i) - \int_{t_s}^{t_e} \lambda(t) dt \tag{7}$$

where t_s and t_e define the starting and the ending time of the activity [*Ogata*, 1993].

[23] Model selection, particularly the determination of the number of parameters, is carried out using the Akaike information criterion (AIC) [*Akaike*, 1974; *Parzen et al.*, 1998]. The statistic AIC = -2 MLL + $2k$ is computed for each of the models fit to the same data, where MLL is the maximum log likelihood value with respect to the parameters, and k is the total number of fitted parameters. In comparing models with different numbers of parameters, addition of the quantity $2k$ roughly compensates for the additional flexibility which the extra parameters provide. The model with the lower AIC value is taken as giving the better choice for forward prediction purposes. Insofar as it depends on the likelihood ratio, the AIC can also be used as a rough guide for testing the model. In testing a model with $k + d$ parameters against a null hypothesis with just k parameters, we take a difference of 2 in AIC values as a rough estimate of significance at the 5% level. An alternative to the Akaike information criterion is the modified version of Schwarz's information criterion, BIC = MLL $-$ $0.5k \ln(N/2\pi)$, where N is the number of events [*Main et al.*,

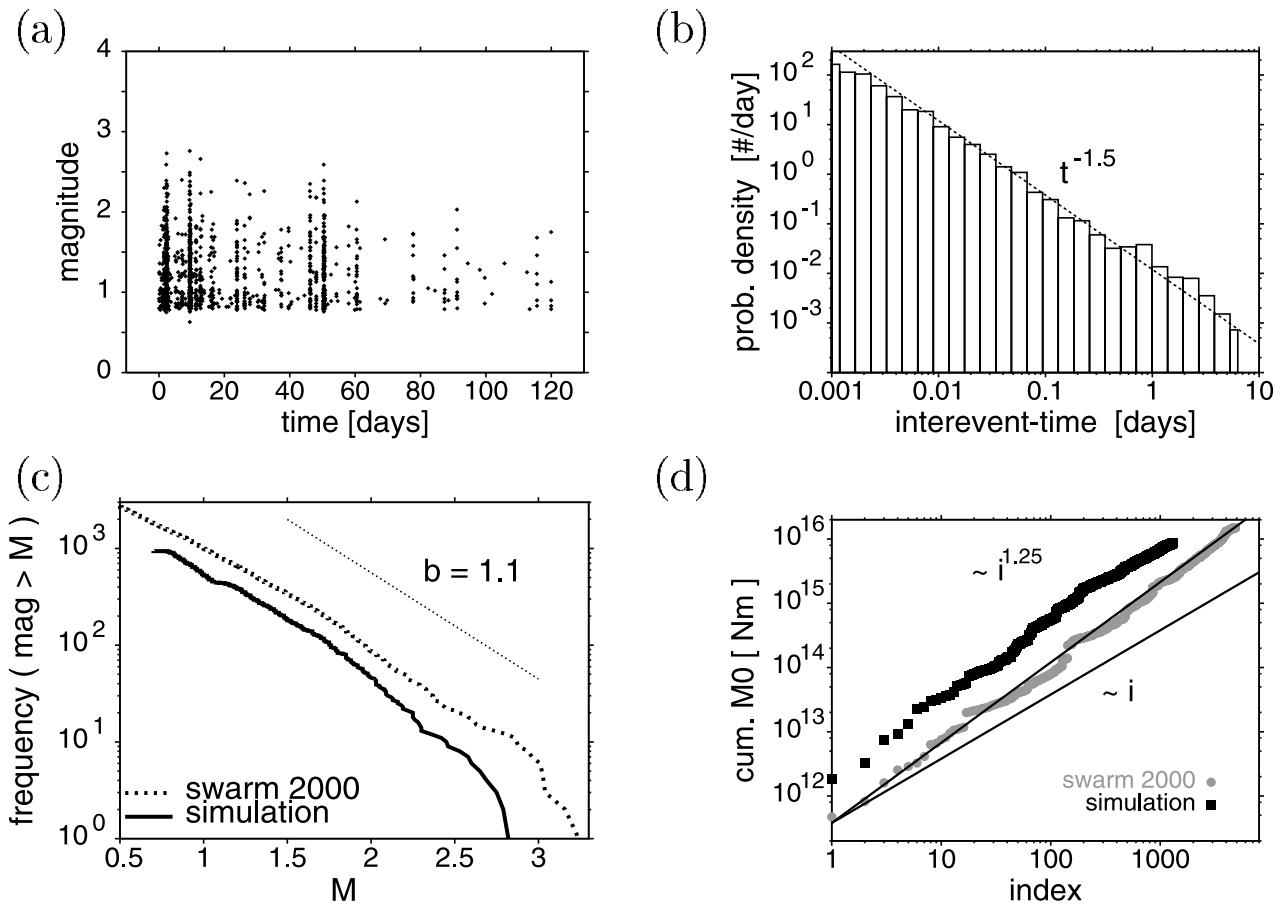

Figure 4. Example of a model simulation: (a) magnitudes as a function of time; (b) interevent time probability distribution; (c) frequency-magnitude distribution; and (d) cumulative seismic moment release as a function of the earthquake index *i*.

1999]. In this case, the best model has the largest BIC value. The BIC criterion has been shown to be superior in the case of larger data sets [*Koehler and Murphree*, 1988].

4.1. Analysis of the Vogtland Earthquake Swarm

[24] The result of the ETAS parameter estimation for the Vogtland earthquake swarm activity is shown in Table 1. The estimated parameters are in agreement with previously observed values for earthquake activity worldwide [*Ogata*, 1992]. In particular, the observed α value for the Vogtland swarm ($\alpha = 0.73$) is similar to previous findings for Japanese earthquake swarm activity, where the α value has been found to scatter in the range [0.35, 0.85], in contrast to nonswarm activity which is characterized by higher values, namely, $\alpha \in [1.2, 3.1]$ [*Ogata*, 1992]. In addition, the table shows the differences of the AIC and BIC value between the ETAS model and a Poissonian (temporally uncorrelated) process, $\Delta AIC = AIC_{ETAS} - AIC_{rand}$ and $\Delta BIC = BIC_{ETAS} - BIC_{rand}$. The negative ΔAIC and positive ΔBIC value indicate that the ETAS model is a better representation of the data. The quality of the fit can be visualized by comparing the expected and the observed number of earthquakes as a function of time. In the case of the ETAS model, we calculate the cumulative number by integration of equation (3). The result is shown in Figure 5. The shape of both curves is almost identical, although there is some shift in the curves which will be later explained.

[25] The fitted ETAS model gives a low forcing rate of about $\lambda_0 = 0.32$ events per day leading to a total of about 38 earthquakes in the whole swarm period of 120 days which means that only 0.8% of all earthquakes are externally triggered. The great majority is self-triggered activity.

[26] In order to find out whether the ETAS model is an appropriate description of the swarm activity and is able to explain the observed fractal interevent time statistics of the Vogtland swarm, we produce Monte Carlo simulations of the ETAS model with the parameters given in Table 1. The simulations are performed by a thinning method using a piecewise constant rates Poisson processes, where the earthquake rate is determined at each time by the preceding earthquakes and the background rate (equation (3)) and

Table 1. Estimated ETAS Parameters of the Vogtland Earthquake Swarm and the Corresponding ΔAIC and ΔBIC Values Quantifying the Quality of the Fit

Parameter	Value
λ_0	0.32
K_0	0.0137
c	0.00046
α	0.73
p	1.37
ΔAIC	−26,098
ΔBIC	13,042

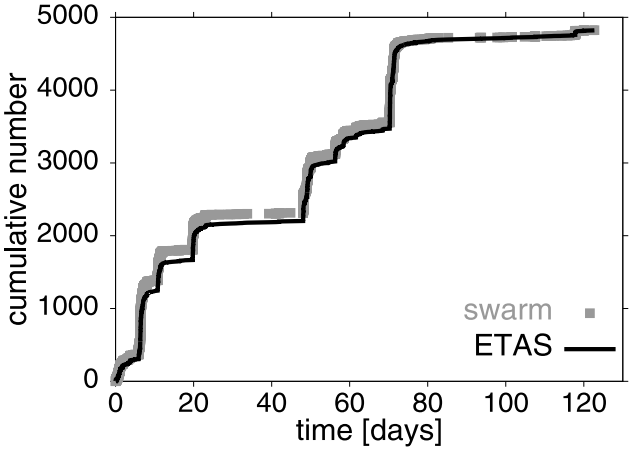

Figure 5. Cumulative number of earthquakes as a function of time observed in the Vogtland swarm compared with that expected by the ETAS model.

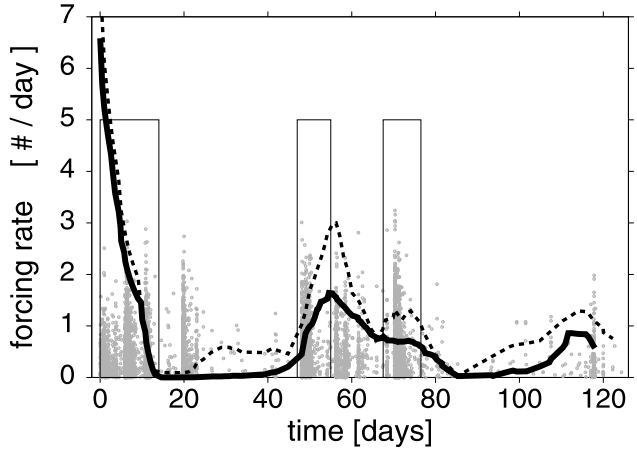

Figure 7. Time dependence of the forcing rate λ_0 resulting from fitting only λ_0 (solid line) or all parameters simultaneously (dotted line), in a moving time window. In addition, the points indicate the analyzed Vogtland earthquake sequence, and the boxes mark the phases in which the spatial spreading indicates pore pressure diffusion [see *Parotidis et al.*, 2003].

magnitudes are taken from the original swarm sequence. For that, we use the algorithm given by *Ogata* [1998]. We end the simulations after the number of earthquakes reaches that of the original catalog. Figure 6a shows a typical example for such a stochastic forward simulation. The synthetic earthquake sequence consists of several subswarms in agreement with the original earthquake swarm. The fine structure is also reproduced by the ETAS simulation. Figure 6b shows the interevent time distribution of the Monte Carlo simulation in comparison with that of the original earthquake swarm. Both distributions are very similar and can be fitted by the same power law $t^{-1.5}$.

4.1.1. Time Dependence of the Forcing Rate

[27] For the simulation shown in Figure 6a, we use the seismic activity of the first 5 swarm days as initial conditions. We find that simulations without any given initial activity show a much slower starting phase compared to the Vogtland swarm. This points to a nonstationary behavior, in particular at the initiation phase. To explore this nonstationary behavior, we fit the ETAS model in a moving time window, the length of which is set to 10 days. We perform the calculation in two alternate ways: (1) only the parameter λ_0 is fitted, where all other parameters are set to the values found for the whole sequence (see Table 1) and (2) all five parameters are fitted in each time window. The latter procedure is more unstable for swarm episodes with a small number of earthquakes. However, the results for both calculations are similar. We find a large systematic variation in the external forcing strength λ_0 (Figure 7). The earthquake swarm seems to be initiated by a strong fluid impulse which decreases within the first 10 days. A second, weaker peak is observed about two months later, which decreases again with time. The curve can be compared with the phases of diffusion-like hypocenter migration marked as boxes in

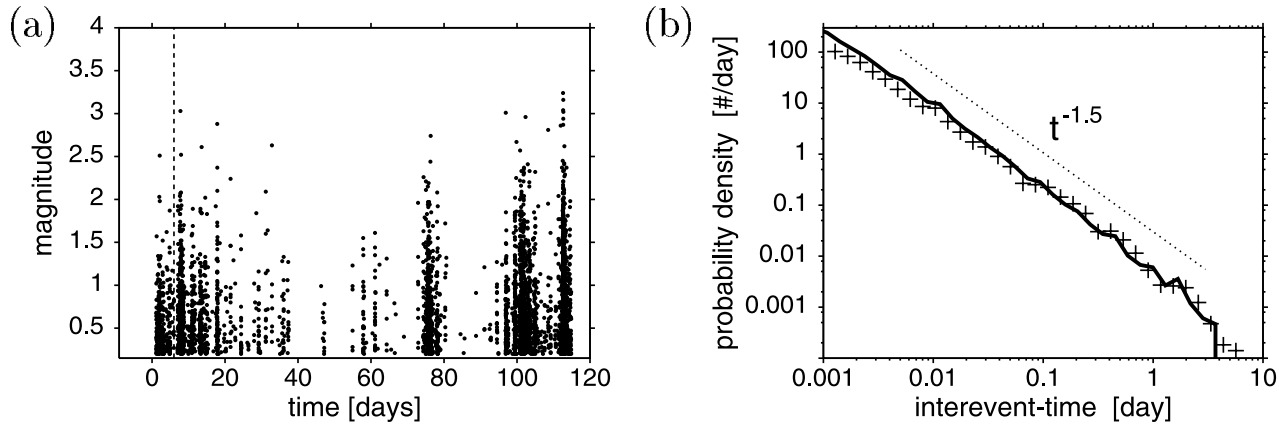

Figure 6. Example of a Monte Carlo simulation of the ETAS model with parameters taken from Table 1. (a) Points representing the magnitudes of the simulated earthquakes as a function of time. The dashed line marks the first 5 days which are taken from the original swarm sequence as initial activity. (b) A log-log plot showing the probability density for observing a certain waiting time between successive earthquakes in the simulated (line) and empirically observed (crosses) swarm activity. Both distributions can be fitted by the same power law $\sim t^{-1.5}$ (dotted line).

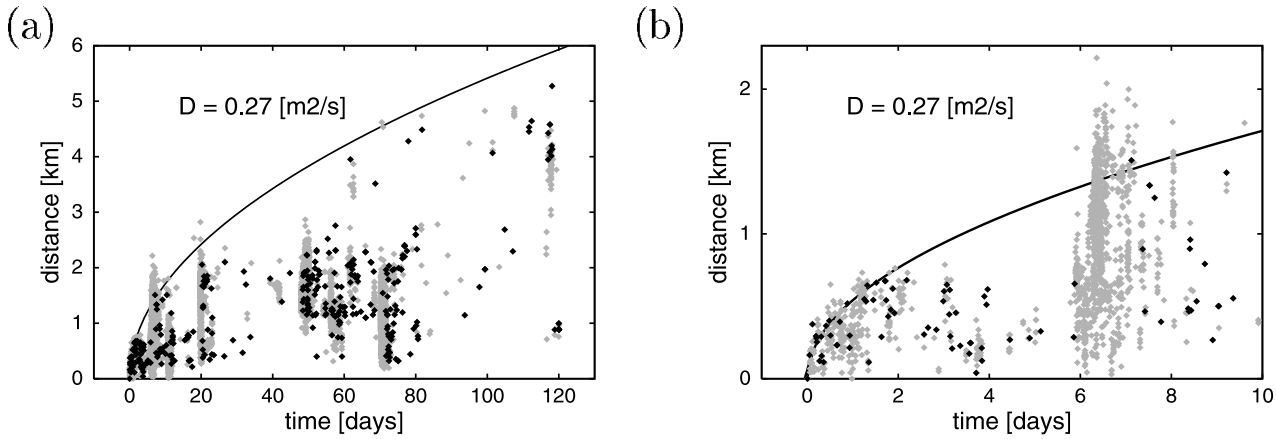

Figure 8. (a) Hypocenter distances measured from the first event as a function of the earthquake occurrence times for the Vogtland swarm (light points are clustered events; dark points are background events). The line refers to the theoretical position of the propagating pore pressure front in the case of a hydraulic diffusivity of $D = 0.27$ m^2/s. (b) Only the first 10 days.

Figure 7. These phases have been previously detected by analyzing the local spreading characteristics within this swarm activity [*Parotidis et al.*, 2003]. Both results correlate. In particular, the large subswarm that occurred after 20 days shows no sign of fluid triggering either in its temporal or in its spatial characteristics. After about 110 days, however, our curve shows a small fluid signal previously not observed.

4.1.2. Declustering Based on ETAS Model

[28] The ETAS modeling can also be used to decluster the earthquake catalog. To begin with, we use the declustering procedure proposed by *Zhuang et al.* [2002]. The probability that an event i belongs to the background is calculated by the ratio between background rate and the total occurrence rate, $\lambda_0/\lambda(t_i)$, where $\lambda(t_i)$ is calculated according to equation (3). Events are assigned to the background on a random basis. We thus obtain different stochastic versions of declustered catalogs by repetition of the procedure. For 1000 versions, we calculate the percentage of background earthquakes. The mean value is 0.8% with a standard deviation of 0.1%. This value is in agreement with our previous estimate.

[29] The declustering procedure does not, however, consider the nonstationary nature of the background rate. To account for this variability, we use the curve $\lambda_0(t)$ (Figure 7) as an input to the declustering procedure. The resulting percentage of background earthquakes is 2.4 ± 0.2%. In addition, we use a simpler procedure which requires no previous knowledge of the nonstationarity. In this case, we calculate for each event whether or not it is likely to be a part of an earthquake cluster by means of the log likelihood ratio, $\Delta = \mathrm{MLL}_{\mathrm{ETAS}} - \mathrm{MLL}_{\mathrm{rand}}$; that is the difference between the maximum log likelihood value of the ETAS model and that of a Poissonian process. This value is computed for the sequence with (Δ_{all}) and without (Δ_{-i}) the event under investigation. In the case $\Delta_{\mathrm{all}} > \Delta_{-i}$, the activity becomes more similar to a Poisson process if the event is not taken into account. Thus the earthquake is part of an earthquake cluster. Vice versa, the event occurred temporally uncorrelated in the case $\Delta_{\mathrm{all}} < \Delta_{-i}$. In this way, we can remove the clustered earthquakes from the catalog.

[30] Applying the latter procedure to the Vogtland earthquake swarm, the catalog is reduced to 342 events (7.1% of the activity). For a comparison, in Figure 8 we show the spatiotemporal distribution of the complete and declustered swarm activity. Here, the distance from the first event of the sequence is plotted as a function of the occurrence time. First, we find that the main clusters have disappeared. Some clustering remains in the time period between 50 and 70 days after the swarm initiation. This is in agreement with our previous finding that the fluid signal is enlarged in this swarm period (see Figure 7). Second, we compare the data points with the theoretical prediction for fluid induced earthquake activity. In the simplest case of fluid diffusion, the distance r of the propagating pore pressure front from the point source is given by $r = \sqrt{4\pi Dt}$ [*Shapiro et al.*, 1997], where t is the time and D the hydraulic diffusivity. The earthquakes are expected to occupy the space beneath this curve. The fit of this theoretical curve is rather poor for the complete catalog, but becomes much better for the declustered data. In the latter case, the previously proposed value of $D = 0.27$ m^2/s [*Parotidis et al.*, 2003] fits the swarm migration well. This indicates that the ETAS modeling in the time domain can also be used to reveal the spatial patterns of the fluid signal.

4.1.3. Discussion

[31] The ETAS modeling can be used in order to identify the background as well as the triggered component of seismicity. Statistical modeling of the Vogtland earthquake swarm has shown that the fractal temporal statistics are solely explainable by the triggered component, namely an epidemic aftershock occurrence, whereas the signal of the external forcing is almost completely buried. Applying a stationary ETAS model, the percentage of background events is estimated to be 0.8 ± 0.1%. Accounting for nonstationary behavior, the two applied declustering procedures yield slightly larger values of about 2.4% and 7.1%, respectively.

[32] The deconvolution of the time dependence of the external forcing signal reveals a dominant forcing signal initiating the swarm activity and a secondary smaller peak after 50 days. For Figure 7, we use an arbitrary value of

Table 2. Estimated ETAS Parameters and Corresponding ΔAIC, ΔBIC Values for Different Model Simulations

Model Simulation	D, m^2/s	x_0, km	ΔP, MPa	T, days	κ	λ_0	K_0	c	α	p	ΔAIC	ΔBIC
a	1	10	2	0.1	0.3	0.34	0.0067	0.0022	2.06	1.48	−7264	3627
b	1	11	2	0.1	0.3	0.75	0.0025	0.0028	1.99	1.73	−7343	3667
c	0.27	10	5	0.5	0.2	0.70	0.0173	0.0022	1.95	1.19	−1878	935
d	0.27	11	5	0.5	0.2	1.10	0.0086	0.0021	2.18	1.29	−1601	798
e	0.1	10	5	0.5	0.3	0.78	0.0120	0.0027	2.07	1.34	−3773	1882
f	0.1	11	5	0.5	0.2	0.55	0.0098	0.0012	1.88	1.28	−570	284

10 days for the moving time window. We find that the time window acts like a filter; in other words, shorter time windows produce additional short period fluctuations and longer time windows smooth the curve. However, the general shape of this λ_0 curve is found to be independent of the chosen time window.

[33] Generally, it cannot be determined whether the background activity results from tectonics or pore pressure changes. However, we are confident that our observed signal is related to fluids because of the large variations on a short timescale which are inexplicable by tectonic causes. In section 4.2 we demonstrate by means of model simulations that the observed temporal variations of the forcing parameter λ_0 are directly correlated with the underlying fluid flows.

4.2. Analysis of Model Simulations

[34] We now repeat the analysis of the Vogtland swarm in section 4.1. First, we fit the ETAS model to the simulated earthquake catalogs in order to deconvolute the stress and the fluid signal. The estimations of the five parameters of the ETAS model (λ_0, K_0, α, c, p) and the differences of the AIC and BIC values between the ETAS model and a Poissonian process are summarized in Table 2 for six different simulations. The values λ_0, K_0, and p are found to scatter in the same range as for the Vogtland swarm (Table 1). Furthermore, the differing values of c and ΔAIC(ΔBIC) can be understood as follows: The larger values of c are likely to result directly from the chosen timescale in equation (5) which yields an afterslip rate proportional to $(1[\text{min}] + \Delta t)^{-1}$. If the rate of aftershocks is proportional to the afterslip rate, then a c value of 1 [min] $\approx$ 0.0007 [days] is expected. Thus a slightly reduced timescale in equation (5) could explain the smaller c value for the Vogtland swarm. The smaller differences of the AIC and BIC values can be explained by the smaller number of earthquakes in the catalogs due to the limited magnitude range. However, the deviation of the parameter α seems to be significant. This value is found to be close to 2 in contrast to 0.73 in the case of the Vogtland swarm. Thus the simulations resemble the α values typical for seismicity at tectonic plate boundaries rather than for swarm activity [*Ogata*, 1992]. Probably, the differing α value indicates that the postseismic creep triggering mechanism overestimates the magnitude dependence found in the swarm activity. Because afterslip is assumed to be proportional to coseismic slip in our model, the stress changes due to the proposed mechanism scale with the seismic moment M_0 of the earthquake. Note that the parameters in Table 2 are estimated for local magnitudes which are calculated from the seismic moment according to $M_L = 0.95 \log(M_0) - 10.76$. Thus a value of $\alpha = \ln 10/0.95 \approx 2.4$ should be observed if $\exp(\alpha M_L) \sim M_0$ is assumed; in this case the aftershock productivity is strictly correlated to the stress changes, particularly M_0. However, the effect of stress changes depends on the Coulomb failure stress field which is dynamically evolving during our model simulations. The stress field evolution explains the slightly reduced value ($\alpha \approx 2.0$), but it cannot explain the discrepancy with the observed value in the Vogtland region. A possible explanation is that we neglect the mechanism of pore creation proposed by *Yamashita* [1999]. This effect is assumed to increase with earthquake magnitude, but would counteract the mechanism of afterslip, because the creation of pore volume results in a drop of pore pressure, thus a decrease of Coulomb failure stress (equation (1)). Therefore afterslip, in combination with pore creation, could explain the lower value of α found for swarm activity.

[35] In the next step, we asses whether the underlying pore pressure change can be recovered by the procedure applied to the Vogtland swarm in section 4.1.1. For that, we fit the ETAS parameter λ_0 in a moving time window of 10 days. All other ETAS parameters are set to the values which are estimated for the whole earthquake sequence. To assess if the deconvolution of stress and fluid signal works, we compare the resulting variation of λ_0 with the spatially averaged rate of pore pressure increase, which is known exactly for these model simulations. Figure 9 shows the result for each of the simulations summarized in Table 2. We find that the deconvolution works well. Despite some fluctuations, the main shape of the fluid signal is reproduced in all cases. Furthermore, not only the shape but also the absolute values of λ_0 are correlated with the strength of the pore pressure increase. Note that we have arbitrarily set the time window to 10 days for both the analysis of the simulations and the Vogtland swarm. Optimization of the time window will probably be able to clarify the results.

5. Summary and Conclusion

[36] Two mechanism are often assumed to cause earthquake clustering: stress triggering and fluid flow. Whereas stress triggering can be tackled sometimes in isolation, e.g., in the case of undrained rocks, fluid induced seismic activity will always incorporate both mechanisms. Thus stress triggering can dominate seismicity patterns, although it is not the initial process. We find that this is the case for swarm activity in the Vogtland region. The stress triggering signal which is identified with Omori-like aftershock sequences dominates the whole activity. The epidemic type aftershock sequence (ETAS) model fits the earthquake sequence very well. Only a few percent of the activity is found to be directly triggered by the fluid signal. The temporal evolution of the fluid signal is revealed by fitting

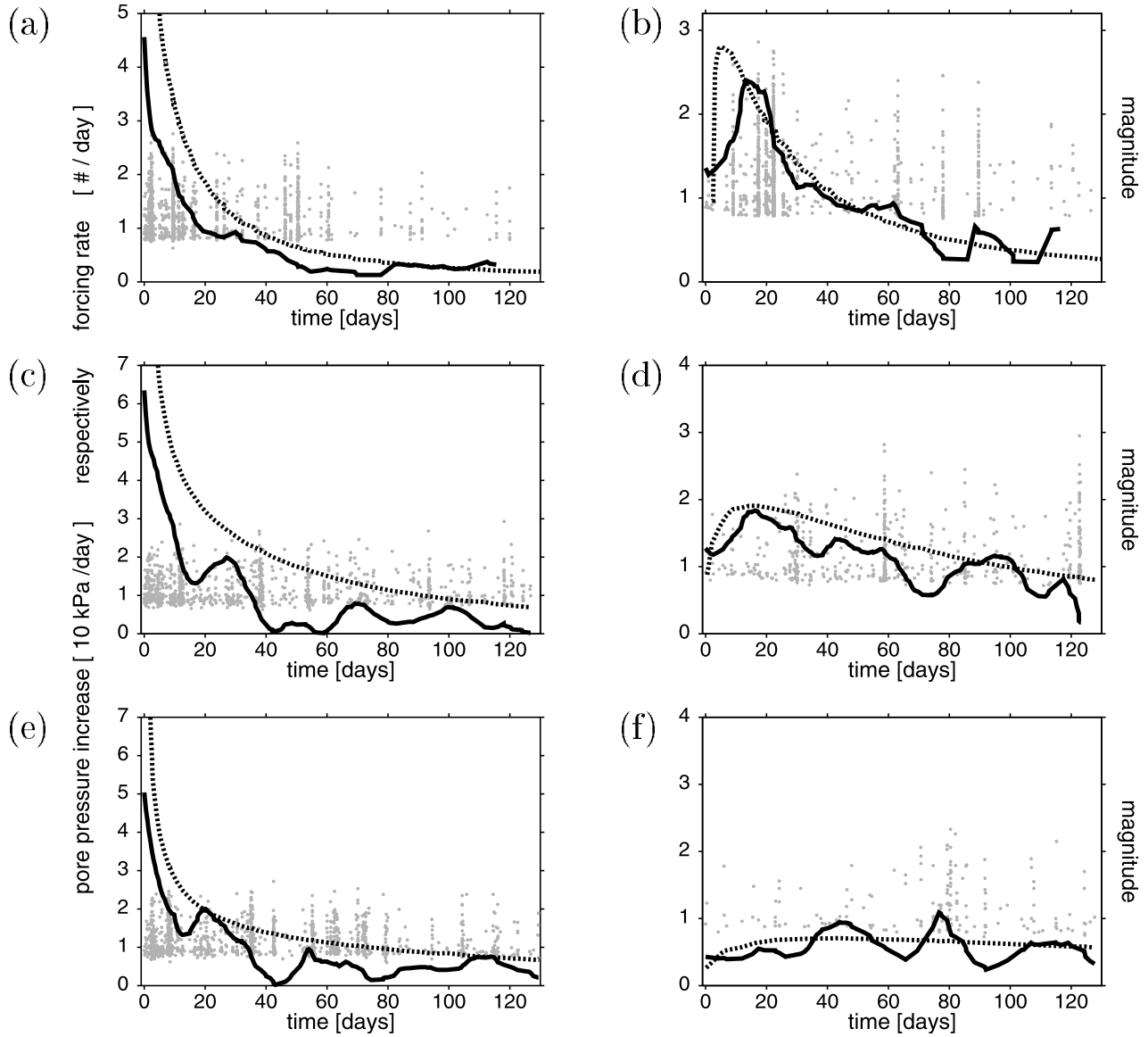

Figure 9. For each of the model simulations a–f in Table 2, Figures 9a–9f show the time dependence of the forcing rate λ_0 resulting from fitting λ_0 (solid line) in a moving time window. In each case, this curve is compared with the really underlying rate of pore pressure increase (dashed line). The points refer to the analyzed earthquakes.

the ETAS model in moving time windows. We find a clear indication for fluids initiating the swarm activity within the first days. Afterward only a smaller secondary peak is observed during the swarm evolution. This finding is in agreement with the previously observed nonfractal temporal clustering characteristics in the initiation phase [*Hainzl and Fischer*, 2002] and observations related to hypocenter diffusion [*Parotidis et al.*, 2003]. The pattern of hypocenter diffusion itself is shown to be resolved by an ETAS-based declustering of the earthquake catalog. Note that the proposed method analyzes solely earthquake sequences and make no use of hypocenter information.

[37] The efficiency of the deconvolution procedure is proved by an analogous analysis of simulated earthquake activity, which is forced by pore pressure diffusion and incorporates stress field changes in a three-dimensional elastic half-space. The statistical characteristics of these simulations are in good agreement with the Vogtland earthquake swarm; in particular, the magnitudes and the interevent times are distributed in a very similar way. Although the most conspicuous seismicity patterns of these simulations result from stress triggering, we find that our deconvolution procedure is able to reconstruct the buried fluid signal in its main parts. Thus this procedure seems to be a promising method to unveil fluid signals in seismicity patterns, even in the case of poor hypocenter information.

[38] **Acknowledgments.** The authors wish to thank Andrea Antonioli, Ian Main, and Sandy Steacy for their recommendations which helped us to improve this paper significantly. Furthermore, we are thankful to Tomas Fischer and Lindsay Schoenbohm for stimulating discussions and discerning reading of the manuscript. S.H. was supported by the Deutsche Forschungsgemeinschaft (SCH280/13-2).

References

Akaike, H. (1974), A new look at the statistical model identification, *IEEE Trans. Autom. Control*, *AC-19*, 716–723.

Ben-Zion, Y., and J. R. Rice (1993), Earthquake failure sequences along a cellular fault zone in a three-dimensional elastic solid containing asperity and nonasperity regions, *J. Geophys. Res.*, *98*, 14,109–14,131.

Brauer, K., H. Kampf, G. Strauch, and S. M. Weise (2003), Isotopic evidence ($^3He/^4He$, $^{13}C_{CO_2}$) of fluid-triggered intraplate seismicity, *J. Geophys. Res.*, *108*(B2), 2070, doi:10.1029/2002JB002077.

Burgmann, R., S. Ergintav, P. Segall, E. H. Hearn, S. McClusky, R. E. Reilinger, H. Woith, and J. Zschau (2002), Time-dependent distributed afterslip on and deep below the Izmit earthquake rupture, *Bull. Seismol. Soc. Am.*, *92*, 126–137.

Dieterich, J. (1972), Time-dependent friction in rocks, *J. Geophys. Res.*, *77*, 3690–3697.

Fischer, T. (2003), The August–December 2000 earthquake swarm in NW Bohemia: the first results based on automatic processing of seismograms, *J. Geodyn.*, *35*, 59–81.

Hainzl, S. (2003), Self-organization of earthquake swarms, *J. Geodyn.*, *35*, 157–172.

Hainzl, S. (2004), Seismicity patterns of earthquake swarms due to fluid intrusion and stress triggering, *Geophys. J. Int.*, *159*, 1090–1096.

Hainzl, S., and T. Fischer (2002), Indications for a successively triggered rupture growth underlying the 2000 earthquake swarm in Vogtland/NW Bohemia, *J. Geophys. Res.*, *107*(B12), 2338, doi:10.1029/2002JB001865.

Hainzl, S., and G. Zöller (2001), The role of disorder and stress concentration in nonconservative fault systems, *Physica A*, *294*, 67–84.

Harris, R. (1998), Introduction to special section: Stress triggers, stress shadows, and implications for seismic hazard, *J. Geophys. Res.*, *103*, 24,347–24,358.

Helmstetter, A., and D. Sornette (2002), Subcritical and supercritical regimes in epidemic models of earthquake aftershocks, *J. Geophys. Res.*, *107*(B10), 2237, doi:10.1029/2001JB001580.

Horalek, J., T. Fischer, A. Bouskova, and P. Jedlicka (2000), Western Bohemia/Vogtland in the light of the WEBNET network, *Stud. Geophys. Geod.*, *44*, 107–125.

Jentzsch, G., M. Korn, and A. Spicak (2003), The swarm earthquakes in the area Vogtland/NW-Bohemia: Interaction of tectonic stress and fluid migration in a magmatic environment, *J. Geodyn.*, *35*, 1–3.

Koehler, A. B., and E. S. Murphree (1988), A comparison of Akaike and Schwarz criteria for selecting model order, *Appl. Stat.*, *37*, 187–195.

Kurz, J. H., T. Jahr, and G. Jentzsch (2003), Geodynamic modelling of the recent stress and strain field in the Vogtland swarm earthquake area using the finite-element-method, *J. Geodyn.*, *35*, 247–258.

Main, I. G., T. Leonard, O. Papasouliotis, C. G. Hatton, and P. G. Meredith (1999), One slope or two? Detecting statistically significant breaks of slope in geophysical data, with application to fracture scaling relationships, *Geophys. Res. Lett.*, *26*, 2801–2804.

Nur, A. (1974), Matsushiro, Japan earthquake swarm: Confirmation of the dilatancy-fluid diffusion model, *Geology*, *2*, 217–221.

Ogata, Y. (1988), Statistical models of point occurrences and residual analysis for point processes, *J. Am. Stat. Assoc.*, *83*, 9–27.

Ogata, Y. (1992), Detection of precursory relative quiescence before great earthquakes through a statistical model, *J. Geophys. Res.*, *97*, 19,845–19,871.

Ogata, Y. (1993), Fast likelihood computation of epidemic type aftershock-sequence model, *Geophys. Res. Lett.*, *20*, 2143–2146.

Ogata, Y. (1998), Space-time point-process models for earthquake occurrences, *Ann. Inst. Stat. Math.*, *50*, 379–402.

Okada, Y. (1992), Internal deformation due to shear and tensile faults in a half-space, *Bull. Seismol. Soc. Am.*, *82*, 1018–1040.

Parotidis, M., E. Rothert, and S. A. Shapiro (2003), Pore-pressure diffusion: A possible triggering mechanism for the earthquake swarms 2000 in Vogtland/NW-Bohemia, central Europe, *Geophys. Res. Lett.*, *30*(20), 2075, doi:10.1029/2003GL018110.

Parzen, E., K. Tanabe, and G. Kitagawa (Eds.) (1998), *Selected Papers of Hirotugu Akaike*, Springer, New York.

Ruina, A. L. (1983), Slip instability and state variable friction laws, *J. Geophys. Res.*, *88*, 10,359–10,370.

Scholz, C. H. (1998), Earthquakes and friction laws, *Nature*, *391*, 37–42.

Scholz, C. H. (2002), *The Mechanics of Earthquakes and Faulting*, Cambridge Univ. Press, New York.

Scholz, C. H., and T. Engelder (1976), Role of asperity indentation and ploughing in rock friction, *Int. J. Rock Mech. Min. Sci.*, *13*, 149–154.

Shapiro, S. A., E. Huenges, and G. Borm (1997), Estimating the crust permeability from fluid-injection-induced seismic emission at the KTB site, *Geophys. J. Int.*, *131*, F15–F18.

Stein, R. S. (1999), The role of stress transfer in earthquake occurrence, *Nature*, *402*, 605–609.

Utsu, T., Y. Ogata, and R. S. Matsu'ura (1995), The centenary of the Omori formula for a decay law of aftershock activity, *J. Phys. Earth*, *43*, 1–33.

Weinlich, F. H., K. Brauer, H. Kampf, G. Strauch, J. Tesar, and S. M. Weise (1999), An active subcontinental mantle volatile system in the western Eger rift, central Europe: Gas flux, isotopic (He, C, N) and compositional fingerprints, *Geochim. Cosmochim. Acta*, *63*, 3653–3671.

Yamashita, T. (1997), Mechanical effect of fluid migration on the complexity of seismicity, *J. Geophys. Res.*, *102*, 17,797–17,806.

Yamashita, T. (1998), Simulation of seismicity due to fluid migration in a fault zone, *Geophys. J. Int.*, *132*, 674–686.

Yamashita, T. (1999), Pore creation due to fault slip in a fluid-permeated fault zone and its effect on seismicity: generation mechanism of earthquake swarm, *Pure Appl. Geophys.*, *155*, 625–647.

Zhuang, J., Y. Ogata, and D. Vere-Jones (2002), Stochastic declustering of space-time earthquake occurrences, *J. Am. Stat. Assoc.*, *97*, 369–380.

S. Hainzl, Institute of Geo Sciences, University of Potsdam, D-14415 Potsdam, Germany. (hainzl@geo.uni-potsdam.de)

Y. Ogata, Institute of Statistical Mathematics, Tokyo, 106-8569 Japan. (ogata@ism.ac.jp)